Observability-based Local Path Planning and Collision Avoidance Using Bearing-only Measurements

Huili Yu[a], Rajnikant Sharma[a], Randal W. Beard[a], Clark N. Taylor[b]

[a]*Department of Electrical and Computer Engineering, Brigham Young University, Provo, Utah, 84602*
[b]*Sensors Directorate, Air Force Research Labs, USA*

Abstract

In this paper we present an observability-based local path planning and collision avoidance technique. Bearing-only measurements are utilized to estimate the time-to-collision (TTC) and bearing to obstacles using an extended Kalman Filter (EKF). To ensure the error covariance matrix computed by an EKF is bounded, the system should be observable. We perform a nonlinear observability analysis to obtain the necessary conditions for complete observability. We use these conditions to design a path planning algorithm that enhances observability while avoiding collisions with obstacles. We analyze the behavior of the path planning algorithm and specially define the environments where the path planning algorithm will guarantee collision-free paths that lead to a goal configuration. Numerical results show that the planning algorithm successfully solves the single and multiple obstacle avoidance

Email addresses: huiliyu.yhl@gmail.com (Huili Yu), raj.drdo@gmail.com (Rajnikant Sharma), beard@byu.edu (Randal W. Beard), clark.n.taylor@gmail.com (Clark N. Taylor)

Report Documentation Page

Form Approved
OMB No. 0704-0188

1. REPORT DATE	2. REPORT TYPE	3. DATES COVERED
20 JAN 2012		**00-00-2012 to 00-00-2012**

4. TITLE AND SUBTITLE	5a. CONTRACT NUMBER
Observability-based Local Path Planning and Collision Avoidance Using Bearing-only Measurements	5b. GRANT NUMBER
	5c. PROGRAM ELEMENT NUMBER
6. AUTHOR(S)	5d. PROJECT NUMBER
	5e. TASK NUMBER
	5f. WORK UNIT NUMBER
7. PERFORMING ORGANIZATION NAME(S) AND ADDRESS(ES) **Brigham Young University,Department of Electrical and Computer Engineering,Provo,UT,84602**	8. PERFORMING ORGANIZATION REPORT NUMBER
9. SPONSORING/MONITORING AGENCY NAME(S) AND ADDRESS(ES)	10. SPONSOR/MONITOR'S ACRONYM(S)
	11. SPONSOR/MONITOR'S REPORT NUMBER(S)

12. DISTRIBUTION/AVAILABILITY STATEMENT
Approved for public release; distribution unlimited

13. SUPPLEMENTARY NOTES

14. ABSTRACT

In this paper we present an observability-based local path planning and collision avoidance technique. Bearing-only measurements are utilized to estimate the time-to-collision (TTC) and bearing to obstacles using an extended Kalman Filter (EKF). To ensure the error covariance matrix computed by an EKF is bounded, the system should be observable. We perform a nonlinear observability analysis to obtain the necessary conditions for complete observability. We use these conditions to design a path planning algorithm that enhances observability while avoiding collisions with obstacles. We analyze the behavior of the path planning algorithm and specially define the environments where the path planning algorithm will guarantee collision-free paths that lead to a goal configuration. Numerical results show that the planning algorithm successfully solves the single and multiple obstacle avoidance problems while improving the estimation accuracy.

15. SUBJECT TERMS

16. SECURITY CLASSIFICATION OF:			17. LIMITATION OF ABSTRACT	18. NUMBER OF PAGES	19a. NAME OF RESPONSIBLE PERSON
a. REPORT **unclassified**	b. ABSTRACT **unclassified**	c. THIS PAGE **unclassified**	**Same as Report (SAR)**	**33**	

problems while improving the estimation accuracy.

Keywords: Path planning, Collision avoidance, Observability, Miniature Air Vehicle

1. Introduction

Small and Miniature Air Vehicles (MAVs) have the potential to perform tasks that are too difficult or dangerous for human pilots. For example, they can monitor critical infrastructure and real-time disasters, perform search and rescue, and measure weather in-storms [1]. For many of these applications, MAVs are required to navigate in urban or unknown terrain where obstacles of various types and sizes may hinder the success of the mission. MAVs must have the capability to autonomously plan paths that do not collide with buildings, trees or other obstacles. Therefore, the path planning and obstacle avoidance problems for MAVs have received significant attention [1, 2, 3, 4, 5].

The path planning problem can be grouped into global path planning and local path planning. Global path planning requires complete knowledge about the environment and a static terrain. In that setting a collision-free path from the start to the destination configuration is generated before the vehicle starts its motion [6]. The global path planning problem has been addressed by many researchers with common solutions being potential fields methods, roadmap methods and cell decomposition methods [7]. On the other hand, local path planning is executed in real-time during flight. The basic idea is to first sense the obstacles in the environment and then determine a collision-free path [1].

Local path planning algorithms require sensors to detect obstacles. Among the suite of possible sensors, a video camera is cheap and lightweight and fits the physical requirements for small UAVs [1]. However, because of projective geometry, a monocular camera really only measures the bearing to the object. TTC can be estimated by considering the change in the size of the object in the image plane, but this estimate relies on accurately segmenting the image, which can be a noisy process. Therefore, it is a reasonable engineering choice to consider a monocular camera as a bearing-only measurement device and use the camera to estimate both TTC and bearing. We use an extended Kalman Filter (EKF) to extract TTC from bearing measurements.

The key idea presented in this paper is to maneuver the MAV to minimize the state estimation uncertainty while simultaneously avoiding obstacles. We will show that these two tasks are complementary. We use the local mapping technique in our previous work [8, 9, 10], which builds a polar map in the local-level frame of the MAV using the camera measurements directly without transforming to the inertial frame. However, instead of using both TTC and bearing measurements as in [8, 9, 10], in this work we only use bearing measurements to estimate both the TTC and bearing to obstacles. For this purpose we will use the nonlinear observability theory developed by Hermann and Krener [11].

Observability is a measure of information available for state estimation. Song et al. [12] show that the EKF is a quasi-local asymptotic observer for discrete-time nonlinear systems, and that the convergence and boundedness of the filter are achieved when the system satisfies the nonlinear observability rank condition and when the states stay within a convex compact domain.

Observability analysis has been studied extensively for the purpose of estimation [13, 14, 15]. While Bryson and Sukkarieh [16] perform the observability analysis of SLAM and develop an active control algorithm, the observability analysis is not used to develop active control. The contribution of this paper is that we use the observability analysis to explicitly design the path planning algorithm. The initial results of the planning algorithm are presented in [17]. This paper extends the initial results by conducting analysis of the collision avoidance and goal reaching behaviors of the planning algorithm. The main contributions of this paper are as follows:

- We build polar maps using the TTC, which are independent of the ground or air speed of the MAV.
- We perform an observability analysis of the state estimation process from bearing-only measurements and find the necessary conditions for observability of the system.
- We design a path planning algorithm based only on the local map around the MAV in the local-level frame.
- The algorithm minimizes the uncertainties in the TTC and bearing estimates while simultaneously avoiding obstacles.
- We analyze the behavior of the path planning algorithm and determine the class of environments where the algorithm guarantees collision-free paths that maneuver the MAV to a goal configuration.

The paper is organized as follows. Section 2 describes the model of the vehicle in the local-level frame and details a nonlinear observability analysis.

In Section 3 we describe the observability-based path planning algorithm. Section 4 analyzes the behavior of the path planning algorithm. Numerical results are provided in Section 5, and our conclusions are in Section 6.

2. Observability analysis of state estimation

In this section we will build a local map using the TTC to obstacles in the local-level frame of the MAV. The map is constructed in polar coordinates by estimating the TTC and bearing to obstacles. We perform a nonlinear observability analysis of the state estimation problem using bearing-only measurements, find necessary conditions for complete observability of the system, and establish a link between estimation accuracy and collision avoidance.

We assume the MAV is flying at a constant height above ground level and assume obstacles in the environment are static. Since the obstacle map is in the local-level frame of the MAV, the equations of motion of each obstacle relative to the MAV need to be derived. The origin of the local-level frame is the MAV's center of mass. The x-axis points out the nose of the airframe when the airframe is not pitching, the y-axis points out the right wing when the airframe is not rolling, and the z-axis points into the Earth. Throughout the paper, we will assume the zero wind conditions. Let V represent the ground speed of the MAV, which is assumed to be available, and let ϕ and ψ represent the roll and heading angles, respectively. Figure 1 shows the motion of the i^{th} obstacle relative to the MAV in the local-level frame, where τ^i is the TTC, η^i is the bearing whose positive direction is defined as the right-handed rotation about the z-axis of the local-level frame, and O^i is the i^{th} obstacle. Based on Fig. 1, the equations of motion of the obstacle relative

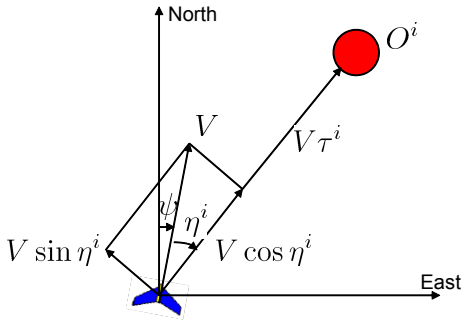

Figure 1: This figure shows the motion of the i^{th} obstacle relative to the MAV. The TTC and bearing to the obstacle are represented by τ^i and η^i. The ground speed is represented by V. The heading angle is represented by ψ. The i^{th} obstacle is represented by O^i.

to the MAV in terms of TTC and bearing are given by

$$\dot{\tau}^i = -\cos \eta^i, \tag{1}$$

$$\dot{\eta}^i = \frac{\sin \eta^i}{\tau^i} - \dot{\psi}, \tag{2}$$

where, assuming coordinated turn conditions, $\dot{\psi} = \frac{g}{V} \tan \phi$ and where ϕ is the roll angle of the MAV, which we assume to be a control signal. Since we use the camera to measure the bearing only (which only requires data association), the measurement at time t is given by

$$z_t^i = \eta_t^i + v_t^i, \tag{3}$$

where v_t^i is the measurement noise that is assumed to be a zero-mean Gaussian random variable. Based on the state transition model expressed by Eqs. (1) and (2) and the observation model expressed by Eq. (3), we use the EKF to estimate the TTC and bearing and we build a TTC map in the local-level frame using polar coordinates, as shown in Fig. 2. The origin of the

map is the current location of the MAV. The circles represent the obstacles and the ellipses around them represent the TTC and bearing uncertainties.

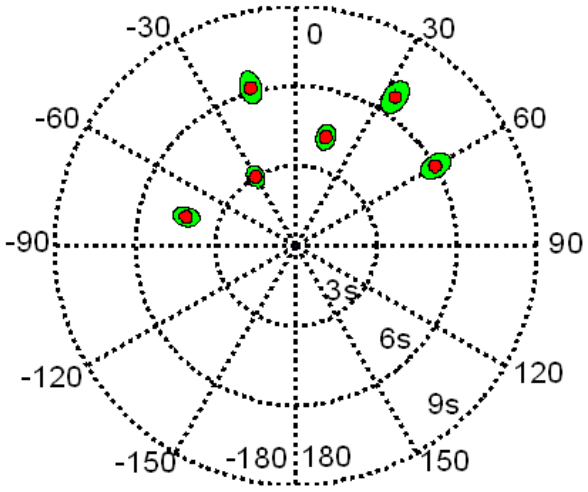

Figure 2: This figure shows the TTC map in the local-level frame of the MAV using polar coordinates. The origin of the map is the current location of the MAV. The circles represent the obstacles and the ellipses around them represent the TTC and bearing uncertainties. The radial direction is TTC in units of seconds.

To decrease the uncertainties in the TTC and bearing estimates, we analyze the observability of the system given by Eqs. (1), (2), and (3). Let $\mathbf{x}^i = [\tau^i, \eta^i]^\top$ represent the state vector associated with the i^{th} obstacle and let $u = \phi$ represent the control input. Let $\dot{\mathbf{x}}^i = \mathbf{f}(\mathbf{x}^i, u)$ represent the state transition model given by Eqs. (1) and (2) and let $z_t^i = h(\mathbf{x}_t^i)$ represent the observation model given by Eq (3). The observability matrix is computed using Lie derivatives described by Hermann and Kerner [11]. The 0^{th} order Lie derivative is $L_{\mathbf{f}}^0(h) = \eta^i$ and the 1^{st} order Lie derivative is $L_{\mathbf{f}}^1(h) = \frac{\partial L_{\mathbf{f}}^0(h)}{\partial \mathbf{x}^i}\mathbf{f} = -\dot{\psi} + \frac{\sin\eta^i}{\tau^i}$. We define the vector of Lie derivatives

$\Omega = [L^0_{\mathbf{f}}(h), L^1_{\mathbf{f}}(h)]^\top$. The observability matrix is computed as

$$\mathbf{O}^i = \frac{\partial \Omega}{\partial \mathbf{x}^i} = \begin{bmatrix} 0 & 1 \\ -\frac{\sin \eta^i}{(\tau^i)^2} & \frac{\cos \eta^i}{\tau^i} \end{bmatrix}. \tag{4}$$

The observability matrix has rank two if and only if $\tau^i \neq \infty$, $\eta^i \neq 2\pi p$ where $p \in \mathbb{Z}$. The EKF is a quasi-local asymptotic observer for nonlinear systems and its convergence and boundedness are achieved when the system is fully observable [12]. Bounds on the EKF error covariance $\mathbf{P}^i$ are related to the observability of the system given by Lemma 1 proved in [12].

Lemma 1 ([12]). *Suppose that there exist positive real scalars* $\alpha_1,\ \alpha_2,\ \beta_1,\ \beta_2$ *such that* $\beta_1 \mathbf{I} \leq {\mathbf{O}^i}^\top \mathbf{O}^i \leq \beta_2 \mathbf{I}$ *and* $\alpha_1 \mathbf{I} \geq \mathbf{C}^i {\mathbf{C}^i}^\top \geq \alpha_2 \mathbf{I}$ *then,*

$$\left(\frac{1}{\beta_2 + \frac{1}{\alpha_2}} \right) \mathbf{I} \leq \mathbf{P}^i \leq \left(\alpha_1 + \frac{1}{\beta_1} \right) \mathbf{I}, \tag{5}$$

where $\mathbf{I}$ *is the identity matrix and* $\mathbf{C}^i$ *is the controllability matrix.*

From Lemma 1, we can see that both the maximum and minimum singular values β_1 and β_2 of the observability matrix should be maximized in order to minimize both the upper and lower bounds of the error covariance matrix. For the problem in this paper the order of the system is two, and therefore minimizing the inverse of the determinant of ${\mathbf{O}^i}^\top \mathbf{O}^i$ will maximize the two eigenvalues of ${\mathbf{O}^i}^\top \mathbf{O}^i$. The determinant of ${\mathbf{O}^i}^\top \mathbf{O}^i$ related to the i^{th}

obstacle is given by

$$\det({\mathbf{O}^i}^\top \mathbf{O}^i) = \frac{\sin^2 \eta^i}{(\tau^i)^4}. \tag{6}$$

From Eq. (6), the inverse of determinant is given by $\frac{(\tau^i)^4}{\sin^2 \eta^i}$. It can be seen that for large τ^i, the inverse is high, which means observability is less, because the change in the bearing measurement is very small with the large TTC (low parallax). It can also be seen that the inverse is minimum at $\eta^i = \pi/2$ and is maximum at $\eta^i = 0$, which means that the vehicle is moving directly toward the obstacle. Minimizing the inverse will ensure that $\eta^i \neq 2p\pi$ and will regulate $\eta^i \to \pi/2$. This implies that the minimization of the inverse of the determinant will minimize the lower and upper bounds of the error covariance matrix as well as steer the MAV away from the obstacle. Therefore the minimization of uncertainty and obstacle avoidance are complementary.

3. Observability-based path planning

Based on the observability analysis in the previous section, we design the observability-based path planning algorithm denoted by π^o such that (a) the uncertainties in the TTC and bearing estimates are minimized and (b) the MAV is maneuvered to the goal configuration. For the objective of goal reaching, the MAV requires knowledge of its own inertial position and the inertial position of the goal. Accordingly, the path planning algorithm π^o requires the use of GPS.

Let τ_t^g and η_t^g represent the TTC and bearing to the goal configuration at time t, and let $\mathbf{x}_t^g = [\tau_t^g, \eta_t^g]^\top$. Let τ_t^i and η_t^i represent the estimated TTC and

bearing to the i^{th} obstacle and let $\mathbf{x}_t^i = [\tau_t^i, \eta_t^i]^\top$. Let $\mathbf{x}_t = [{\mathbf{x}_t^1}^\top, \cdots, {\mathbf{x}_t^n}^\top]^\top$. The determinant of the matrix ${\mathbf{O}^i}^\top \mathbf{O}^i$ associated with the i^{th} obstacle is given by $\det({\mathbf{O}_t^i}^\top \mathbf{O}_t^i) = \frac{\sin^2 \eta_t^i}{(\tau_t^i)^4}$. Let $\nu_t = [{\mathbf{x}_t^g}^\top, {\mathbf{x}_t}^\top]^\top$. Let $\mathcal{I}_t$ represent the index set of all n obstacles and let τ^l represent the maximum TTC to obstacles that the planning algorithm π^o reacts to. Let $\mathcal{B}_t = \{i \in \mathcal{I}_t : \tau_t^i \leq \tau^l, |\eta_t^i| \leq \frac{\pi}{2}\}$ represent the index set of obstacles with the TTC no greater than τ^l and with the azimuth no greater than $\frac{\pi}{2}$. Define the utility function $S : \mathbb{R}^{2n+2} \to \mathbb{R}$ as

$$S(\nu_t) = a_1(\tau_t^g)^2 + a_2(\eta_t^g)^2 + \sum_{i=1}^{n} b_i I_{\mathcal{B}_t}(i) \frac{(\tau_t^i)^4}{\sin^2 \eta_t^i}, \tag{7}$$

where $a_1,\ a_2,\ b_i,\ i = 1, \cdots, n$ are non-negative weights, and $I_{\mathcal{B}_t}(i)$ is the indicator function of the index i, which zeros out the contribution of obstacles that are far away or that are passed by the MAV.

By minimizing the first two terms of Eq. (7), the algorithm drives the MAV towards the goal configuration. The third term penalizes the weighted sum of the inverse of the determinant of ${\mathbf{O}^i}^\top \mathbf{O}^i$ for all obstacles. By minimizing this term, the algorithm achieves two objectives simultaneously. First, it minimizes the uncertainties in the TTC and bearing estimates. Second, the MAV is steered around the obstacles. It is important to note that these two objectives are complementary to each other. We use a look-ahead policy over the horizon T to design the path planner π^o. The cost function to be minimized is given by

$$J = \int_t^{t+T} S(\nu_\rho) d\rho, \tag{8}$$

subject to the constraints

$$\begin{aligned} \dot{\mathbf{x}}_\rho^g &= \mathbf{f}(\mathbf{x}_\rho^g, u_\rho), \\ \dot{\mathbf{x}}_\rho^i &= \mathbf{f}(\mathbf{x}_\rho^i, u_\rho),\ i = 1, \cdots, n, \\ |u_\rho| &\leq \phi_{\max}. \end{aligned} \tag{9}$$

To solve the constrained optimization problem, we discretize the time horizon T as the m-step look-ahead horizon $\{t, t + \Delta t, \cdots, t + m\Delta t\}$, where $\Delta t = T/m$. Equation (8) then becomes

$$J = \sum_{j=1}^{m} S(\nu_{t+j\Delta t}). \tag{10}$$

The optimal path over the m-step look-ahead horizon is found using the nonlinear optimization function fmincon in MATLAB [18] and is replanned once the MAV has followed the first portion of the m-step look-ahead path.

4. Analysis

The utility function given by Eq. (7) can be decomposed as the sum of

$$S_1(\mathbf{x}_t^g) = a_1(\tau_t^g)^2 + a_2(\eta_t^g)^2, \tag{11}$$

and

$$S_2(\mathbf{x}_t) = \sum_{i=1}^{n} b_i I_{\mathcal{B}_t}(i) \frac{(\tau_t^i)^4}{\sin^2 \eta_t^i}. \tag{12}$$

Accordingly, the observability-based path planner π^o that minimizes Eq. (8) can be decomposed into the goal reaching planner denoted by π^g that maneuvers the MAV to the goal by minimizing the cost function

$$J_1 = \int_t^{t+T} S_1(\mathbf{x}_\rho^g) d\rho, \tag{13}$$

and the collision avoidance planner denoted by π^c that maximizes the observability of the system by minimizing the cost function

$$J_2 = \int_t^{t+T} S_2(\mathbf{x}_\rho) d\rho. \tag{14}$$

Remark 1. *We decompose the observability-based path planner π^o into the collision avoidance planner π^c and the goal reaching planner π^g to simplify the analysis of collision avoidance and goal reaching behaviors.*

Accordingly, we analyze the obstacle avoidance behavior of the collision avoidance planner π^c that maximizes the observability of the system and describe under what environment π^c guarantees collision-free paths. We also describe under what environment the collision avoidance planner π^c is guaranteed to drive the MAV to the goal when it is combined with the goal reaching planner π^g.

4.1. Collision avoidance

We analyze the behavior of the collision avoidance planner π^c for avoiding circular obstacles. The collision avoidance planner π^c minimizes the cost

function given by (14) subject to constraints

$$\dot{\mathbf{x}}_\rho^i = \mathbf{f}(\mathbf{x}_\rho^i, u_\rho),\ i = 1, \cdots, n, \tag{15}$$

$$V\tau_\rho^i \geq r^i, i = 1, \cdots, n, \tag{16}$$

where r^i is the radius of the i^{th} obstacle. To guarantee to avoid a single circular obstacle, it is necessary to establish a minimum turn away distance $d_{\min}$ from the obstacle. Let $\phi_{\max}$ represent the maximum roll angle of the MAV and let g represent the gravity constant. The minimum turning radius is then given by [19]

$$r_{mt} = \frac{V^2}{g\tan(\phi_{\max})}. \tag{17}$$

Theorem 1 shows the minimum turn away distance required to avoid a circular obstacle with the radius r using the collision avoidance planner π^c.

Theorem 1. *Using the collision avoidance planner π^c that minimizes the cost function* (14) *subject to the constraints* (15) *and* (16)*, collision avoidance with a circular obstacle with the radius r is guaranteed if the initial condition satisfies*

$$V\tau_0 > d_{\min} = \sqrt{(r + r_{mt})^2 - r_{mt}^2} - r, \tag{18}$$

where τ_0 represents the initial TTC to the circular obstacle. In addition, the MAV converges to a circle around the obstacle with the radius $\max\{r, r_{mt}\}$.

Proof. Consider the worst case scenario where the MAV is flying directly toward a circular obstacle O^i in the local-level frame map, as shown in Fig. 3.

The minimum turn away distance $d_{\min}$ from the obstacle can be determined when the maximum roll angle $\phi_{\max}$ is applied and the generated circle with the minimum turning radius r_{mt} is tangent to the surface of the obstacle. Based on the geometry, the planner π^c is guaranteed to avoid the obstacle if the initial condition satisfies $V\tau_0 > d_{\min} = \sqrt{(r + r_{mt})^2 - r_{mt}^2} - r$.

To show that the trajectory converges to an orbit around the obstacle, if $V\tau_0 > d_{\min}$, the collision avoidance planner π^c will cause the MAV to move in such a way that the TTC to the obstacle decreases and the bearing to the obstacle increases. The MAV will first reach a configuration at time t where the bearing to the obstacle $\eta_t = \frac{\pi}{2}$ and the range to the obstacle $V\tau_t > r$. Then the planner π^c will further cause the MAV to reach a configuration at time t' such that $\eta_{t'} = \frac{\pi}{2}$ and $V\tau_t > V\tau_{t'} > r$. This process is repeated such that the TTC decreases progressively. Because of the constraints (16) on the TTC and the minimum turning radius constraint, the MAV converges to $\max\{r, r_{mt}\}$. □

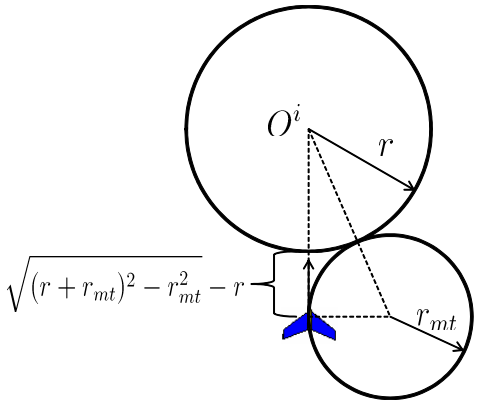

Figure 3: This figure shows the worst case scenario that the MAV is flying directly toward a circular obstacle.

To this point we have found the conditions under which a single circu-

lar obstacle can be successfully avoided using π^c. We extend the analysis to investigate the multiple obstacle avoidance problem. Our approach characterizes the environment with minimum separation between obstacles such that collisions are avoided with all the obstacles.

Let $\mathcal{C}$ represent the configuration space. For two configurations $q_1 = [q_{1n}, q_{1e}, q_{1\psi}]^\top \in \mathcal{C}$ and $q_2 = [q_{2n}, q_{2e}, q_{2\psi}]^\top \in \mathcal{C}$, where q_{in} and q_{ie}, $i = 1, 2$, represent North and East coordinates, and $q_{i\psi}$, $i = 1, 2$, represent the heading angle, define the distance between q_1 and q_2 as

$$\|q_1 - q_2\| \triangleq \sqrt{(q_{1n} - q_{2n})^2 + (q_{1e} - q_{2e})^2}. \tag{19}$$

For a configuration q and the i^{th} obstacle O^i, we define the distance between q and the boundary of O^i as

$$d_q^i \triangleq \min_{q' \in \partial O^i} \|q - q'\|. \tag{20}$$

Let $d^i_{\min}$ and $d^j_{\min}$ represent the minimum turn away distance for the i^{th} obstacle O^i and the j^{th} obstacles O^j given by Eq. (18). Let

$$d^{ij} \triangleq \min_{p_i \in \partial O^i, p_j \in \partial O^j} \|p_i - p_j\| \tag{21}$$

represent the shortest distance between the points along the boundaries of O^i and O^j. Let q_0 represent the initial MAV configuration. Theorem 2 describes the characteristics of the environment in which the collision avoidance planner π^c guarantees collision-free paths.

Theorem 2. *If the environment satisfies* $d^{ij} > \max\{d^i_{\min}, d^j_{\min}\}$, $\forall i, j$ *and*

the initial MAV configuration q_0 *satisfies* $d^i_{q_0} > d^i_{\min}$, $\forall i$, *where* d^{ij} *is the distance between the* i^{th} *and the* j^{th} *obstacles given by Eq.* (21), $d^i_{\min}$ *and* $d^j_{\min}$ *represent the minimum turn away distance for the* i^{th} *and the* j^{th} *obstacles given by Eq.* (18), *and* $d^i_{q_0}$ *is the distance between* q_0 *and the* i^{th} *obstacle given by Eq.* (20), *then the collision avoidance planner* π^c, *which minimizes the cost function* (14) *subject to constraints* (15) *and* (16), *guarantees that the MAV will avoid all obstacles in the future.*

Proof. Consider that the MAV is initially located at q_0 with $d^i_{q_0} > d^i_{\min}$, $\forall i$, and that it will collide with an obstacle O^i if it flies along its initial heading, as shown in Fig. 4. Since $d^i_{q_0} > d^i_{\min}$ and $d^{ij} > \max\{d^i_{\min}, d^j_{\min}\}$, in the worse case scenario the planner π^c leads to a collision-free path from q_0 to q_A on the boundary of O^i with direction tangent to the boundary, where $d^j_{q_A} > d^j_{\min}$. This means that the MAV certainly has the capability to avoid the obstacle O^j when it reaches q_A. In addition, since $d^{jk} > \max\{d^j_{\min}, d^k_{\min}\}$, in the worse case scenario the planner π^c leads to a collision-free path from q_A to q_B on the boundary of O^j with direction tangent to the boundary, where $d^k_{q_B} > d^k_{\min}$. This process can be repeated so that the MAV does not collide with any obstacle using π^c for all time t. □

4.2. Goal reaching

Besides the collision avoidance behavior of the planner π^c, we are also interested in its goal reaching behavior when it is combined with the planner π^g. In this section, we combine the two path planners using a switching algorithm that executes them alternately.

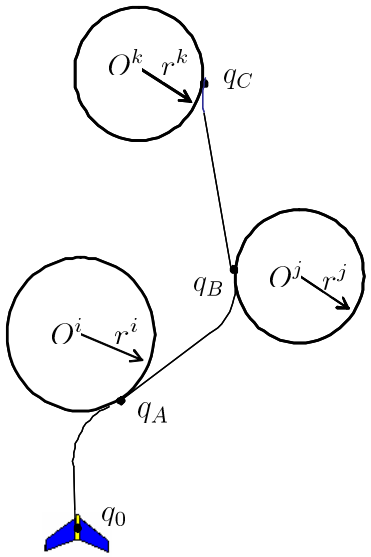

Figure 4: This figure shows the collision avoidance planner π^c maneuvers the MAV to avoid multiple obstacles.

Remark 2. *We analyze the goal reaching behavior of the switching algorithm to simplify the determination of analytical conditions under which the collision avoidance planner π^c is guaranteed to drive the MAV to the goal when it is combined with the goal reaching planner π^g. However, in simulation we use the observability-based planning algorithm π^o that takes into account collision avoidance and goal reaching simultaneously.*

The switching algorithm is described as follows. The algorithm first executes the goal reaching planner π^g to maneuver the MAV toward the goal from an initial configuration. If there exist obstacles with the TTC no greater than τ^l that collide with the MAV, the algorithm executes the collision avoidance planner π^c to react to nearby obstacles. The collision avoidance planner π^c is executed until the MAV reaches a configuration such that the goal reaching planner π^g can generate a path from that configuration to the goal,

which does not collide with any obstacle with TTC less than τ^l. The algorithm then executes the goal reaching planner π^g. This process is repeated until the MAV reaches the goal.

The switching algorithm needs conditions on the environment to ensure that it drives the MAV to the goal. The following theorem describes the conditions under which the MAV can reach the goal from an initial configuration with the heading pointing to the goal using the switching algorithm.

Theorem 3. *If the environment satisfies $d^{ij} > 2V\tau^l$, $\forall i, j$ and the initial MAV configuration q_0 with the heading pointing to the goal satisfies $d^i_{q_0} > d^i_{\min}$, $\forall i$, then the MAV is guaranteed to be maneuvered to the goal using the switching algorithm.*

Proof. Let q_0 represent the initial MAV configuration with the heading pointing to the goal at time t_0 as shown in Fig. 5 and let $d_{t_0} = \|q_0 - q_f\|$ represent the distance between q_0 and q_f. Consider a scenario that there exists an obstacle O^i in the MAV's initial course towards the the goal q_f and that the TTC to the obstacle is no greater than τ^l. For this scenario, since $d^{ij} > 2V\tau^l$, $\forall i, j$, there are no other obstacles with TTC no greater than τ^l when the MAV is located at q_0. The switching algorithm executes the collision avoidance planner π^c to react to the obstacle O^i. Based on Theorem 1, the planner π^c will cause the distance between the MAV and the obstacle O^i to decrease until the MAV converges to a circle with the radius $\max\{r, r_{mt}\}$. This implies that the MAV will stay within the circle C^i centered at O^i with the radius $V\tau^l$, where the planner π^c only reacts to the obstacle O^i until the MAV converges to the circle with the radius $\max\{r, r_{mt}\}$. Accordingly, the switching algorithm executes the collision avoidance planner π^c until the

MAV reaches a configuration q_1 at time t_1 such that the goal reaching planner π^g can generate a path from q_1 to q_f that does not collide with the obstacles O^i. While the MAV flies from q_0 to q_1 using π^c, the bearing to the obstacle O^i is no greater than $\frac{\pi}{2}$. Since the MAV inertial angle to the goal during its flight from q_0 to q_1 is less than the bearing to the obstacle, the inertial angle to the goal must be less than $\frac{\pi}{2}$. Therefore, it must be that $d_{t_1} = \|q_1 - q_f\| < d_{t_0}$.

Once the MAV reaches q_1, the algorithm executes the goal reaching planner π_g until the MAV reaches a configuration q_2 outside of the circle C^i, where another obstacle O^j with TTC no greater than τ^l exists in the MAV's course towards the goal. It is apparent that $d_{t_2} = \|q_2 - q_f\| < d_{t_1}$. Once the MAV reaches q_2, the switching algorithm executes the collision avoidance planner π^c to react to the obstacle O^j. As the process is repeated, the distance between the MAV and the goal decreases progressively and the MAV will be eventually maneuvered to the goal using the switching algorithm. □

The conditions given by Theorem 3 require that each two obstacles in the environment are separated far enough so that the MAV reacts to and avoids obstacles one by one until it reaches the goal. We assume the environment satisfies these conditions in order to provide a theoretical guarantee for the goal reaching behavior of the collision avoidance planner π^c when it is combined with the goal reaching planner π^g. The conditions may not be necessary for the observability-based planning algorithm π^o to achieve goal reaching performance. This implies that there may exist environments that do not satisfy the conditions but where the MAV can still be maneuvered to the goal without causing collisions using π^o.

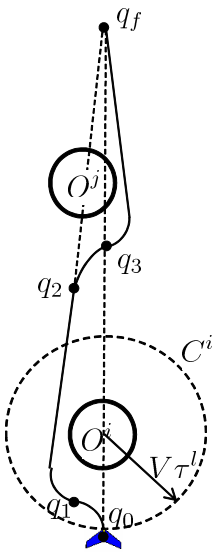

Figure 5: This figure shows the MAV can be maneuvered to q_f using the switching algorithm.

5. Numerical results

In this section, we tested the observability-based planning algorithm π^o that minimizes the cost function (8) and takes into account collision avoidance and goal reaching simultaneously using a simulation environment developed in MATLAB/SIMULINK. The simulator uses a six degree of freedom model of the aircraft. The coordinate system is represented by NED (North-East-Down) system. The covariance matrices of the process and measurement noises were $\mathbf{Q}^i = \begin{pmatrix} 0.001 & 0 \\ 0 & 0.0076 \end{pmatrix}$ and $\mathbf{R}^i = 0.0012$. The weighting scalars a_1 and a_2 were 10 and 1. All the weighting scalars $b_i = 2$, $i = 1, \cdots, n$. A look-ahead policy over a horizon 3.6 seconds was used. The ground speed was $V = 13$ m/s. The maximum roll angle for the MAV was 30°. We tested the algorithm for both single and multiple obstacle avoidance scenarios. We

also conducted Monte Carlo simulations to test the collision avoidance and goal reaching performance of the observability-based planning algorithm π^o with varying measurement uncertainties in the environments with varying minimum distance between obstacles.

5.1. Single obstacle avoidance

In this scenario, the MAV was commanded to maneuver around an obstacle located at (150,250) between waypoint **S** (0,100,-40) and waypoint **E** (600,700,-40) represented by the box and plus signs shown in Fig. 6(a).

Figure 6 shows the path followed by the MAV for avoiding the obstacle using the planning algorithm π^o, the determinant of ${\mathbf{O}^i}^\top \mathbf{O}^i$ for that obstacle, the TTC and bearing, and the TTC and bearing estimation error. It can be seen that when the determinant is maximum, then the bearing is $\eta = \frac{\pi}{2}$ and the TTC reaches its minimum value $\tau_{min} \approx 4$ s. At the same time, the bound on the error covariance for the TTC is minimum, which shows that the uncertainties in state estimates can be minimized while simultaneously avoiding collisions.

5.2. Multiple obstacle avoidance

In the multiple obstacle avoidance scenario, the MAV was commanded to maneuver through twenty-five obstacles between waypoint **S** (0,100,-40) and waypoint **E** (600,700,-40), as shown in the subfigures on the right of Fig. 7.

Figure 7 shows the evolution of the local map in the local-level frame and the update of the path in the inertial frame at different time. The dashed circles in the subfigures on the left represent the TTC at 3 s, 6 s, and 9 s for the inner, middle, and outer circles respectively. The plus sign in

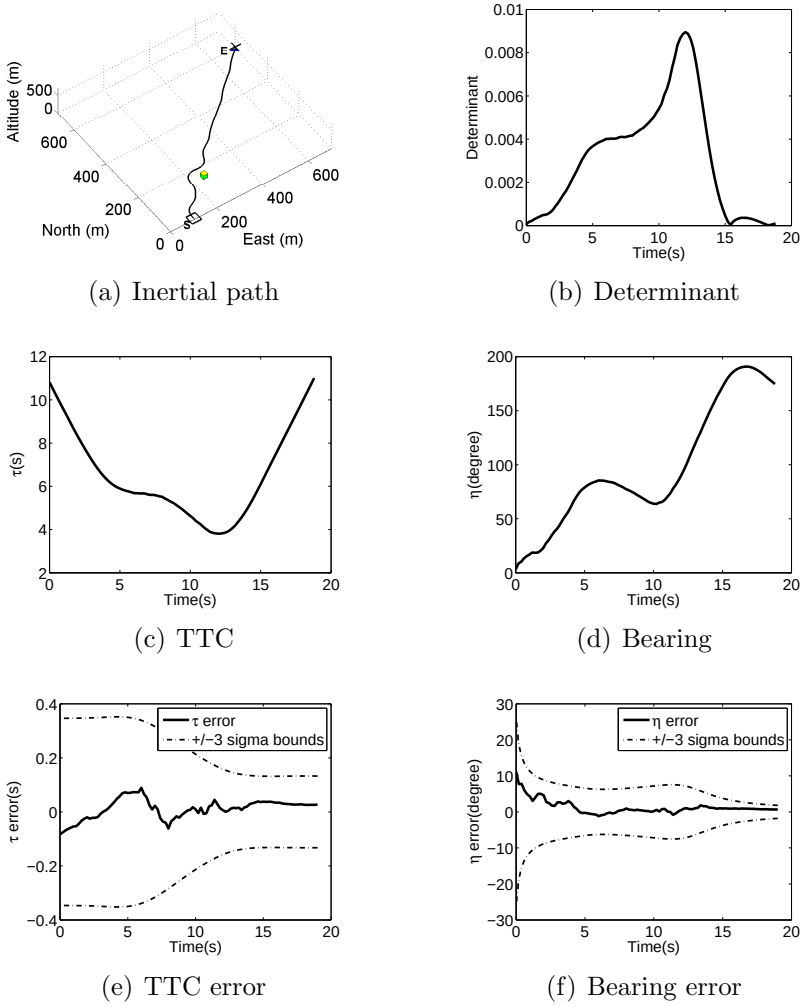

(a) Inertial path (b) Determinant

(c) TTC (d) Bearing

(e) TTC error (f) Bearing error

Figure 6: This figure shows the simulation results for single obstacle avoidance problem. Subfigure (a) shows the inertial path. Subfigure (b) shows the determinant of $\mathbf{O}^{i\top}\mathbf{O}^{i}$. Subfigures (c) and (d) show the TTC and bearing to the obstacle. Subfigure (e) and (f) show the estimation error and $\pm 3\sigma$ bounds of the error covariance for the TTC and bearing.

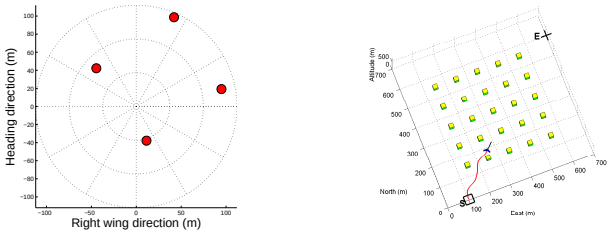

(a) t=20 s

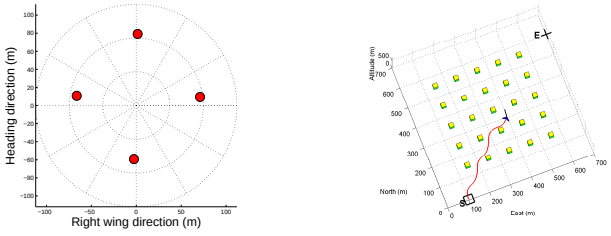

(b) t=35 s

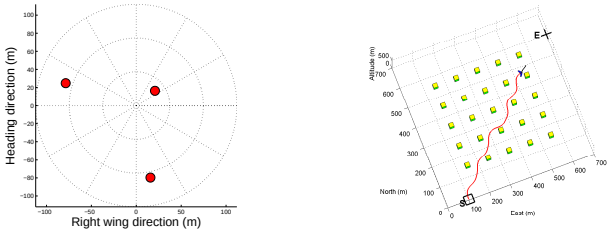

(c) t=53 s

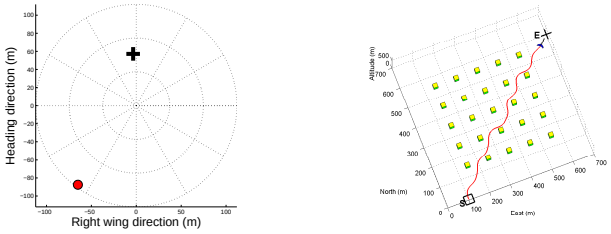

(d) t=65 s

Figure 7: This figure shows the evolution of the local map and the update of the path at different times. Subfigures on the left show the evolution of the local map. The dashed circles represent the TTC at 3 s, 6 s, and 9 s for inner, middle, and outer circles respectively. Subfigures on the right show the path in the inertial frame. The black lines represent the three-step look-ahead paths and red lines represent the actual path followed by the MAV.

subfigure (d) on the left represents the waypoint $\mathbf{E}$ in the local-level frame. Red lines in the subfigures on the right represent the paths followed by the MAV and black lines represent the optimal look-ahead paths. Figure 8 shows the TTC and bearing to the obstacle located at (150,250), the TTC and bearing estimation error, and the determinant of $\mathbf{O}^{i\top}\mathbf{O}^{i}$ for that obstacle. We can see that minimizing the cost function for multiple obstacle avoidance gives the same behavior for the obstacle avoidance, observability and further estimation uncertainties.

Figure 9 shows how the value of the cost function changes as time progresses. Based on the figure, the cost function decreases initially when there are no obstacles in the local map. The cost function only consists of the first term. Once a new obstacle pops up, the cost function increases because the obstacle term is added to the cost function. The planning algorithm π^o then minimizes the second term, causing the cost function to decrease. Once the collision is avoided and the obstacle is passed, it does not add any cost to the cost function. The cost function then decreases based on the first term. Similar behavior occurs when multiple obstacles are observed.

5.3. Monte Carlo simulation

To simplify the analysis of collision avoidance and goal reaching performance and determine analytical conditions, in previous section we decompose the observability-based planning algorithm π^o into the collision avoidance planner π^c and the goal reaching planner π^g. We then analyze of obstacle avoidance behavior of the planner π^c and the goal reaching behavior of the switching algorithm that executes the two planners alternately. Accordingly, the conditions for collision avoidance and goal reaching described in

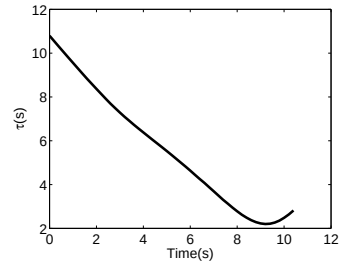

(a) TTC

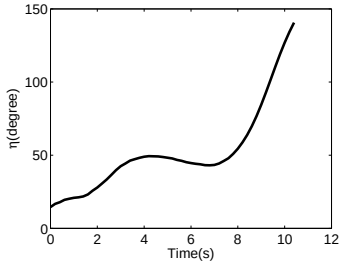

(b) Bearing

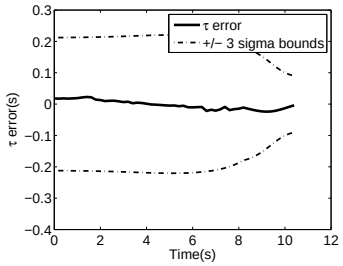

(c) TTC error

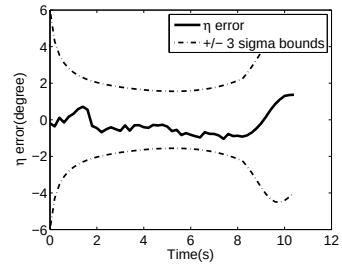

(d) Bearing error

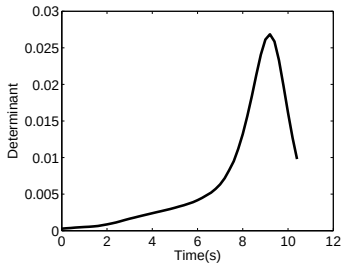

(e) Determinant

Figure 8: This figure shows the TTC and bearing to the obstacle located at (150,250), the TTC and bearing tracking error and the determinant of ${\mathbf{O}^i}^\top \mathbf{O}^i$. Subfigures (a) and (b) show the TTC and bearing. Subfigure (c) and (d) show the error and $\pm 3\sigma$ bounds of the error covariance. Subfigure (e) shows the determinant of ${\mathbf{O}^i}^\top \mathbf{O}^i$.

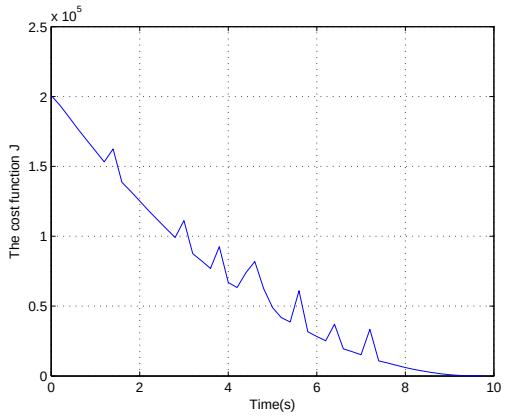

Figure 9: This picture shows the change of the value of the cost function as time progresses.

Theorem 2 and 3 may not be identical for the observability-based planner π^o to achieve collision avoidance and goal reaching performance. Accordingly, we conducted Monte Carlo simulations to demonstrate the statistical performance of the observability-based planning algorithm π^o.

For each environment with a fixed minimum distance between obstacles, we executed 100 simulation runs. In each simulation run, the MAV was maneuvered from the initial position (120,120,-40) to the end position (580,580,-40) through an environment using π^o. The environment was constructed so that each obstacle was added to the environment based on a uniform distribution over the square area with the South-West corner (100,100) and the North-East corner (600,600) until no more obstacles could be added. The height and radius for all obstacles were 100 meters and 20 meters, and the MAV was flying at a height of 40 meters. The observability-based planner π^o reacts to obstacles with TTC no greater than τ^l =4 s. We evaluate two criteria: the number of collisions and the percentage of runs where MAV reached the goal. We say that the MAV reaches the goal if it is maneuvered

to the goal in $t < 100$ seconds without any collisions.

Figure 10 (a) plots the average number of collisions over 100 simulation runs versus the minimum distance between obstacles for the case where the standard deviation of the bearing measurement noise is 2°, as shown by the solid line, and for the case where the locations of obstacles are perfectly known, as shown by the dashed line. The figure shows the average number of collisions decreases dramatically as the minimum distance between obstacles increases from 5 to 20 meters for both cases. After the minimum distance is greater than 20 meters, the average number of collisions decreases slowly for the case with measurement uncertainties and the average number of collisions is zero for the case where the locations of obstacles are perfectly known. The results match the obstacle avoidance behavior of the collision avoidance planner π^c. Given $V = 13$ m/s, $\phi_{\max} = 30°$, and $R_i = 20$ m, $\forall i$, the minimum distance satisfying the obstacle avoidance conditions of Theorem 2 for the planner π^c is 19.9345 meters. When the minimum distance is less than 19.9345 meters, the number of collisions decreases quickly as the minimum distance increases. When the minimum distance is greater than 19.9345 meters, the conditions of Theorem 2 are satisfied. The collision avoidance planner π^c guarantees collision-free paths if the obstacle locations are perfectly known. For the case with the measurement uncertainties, the MAV still encounters a small number of collisions when the minimum distance is greater than 20 meters. In addition, when the minimum distance is 10 and 15 meters for the case with perfectly known obstacle locations, the average number of collisions is less than one, which implies that there exist environments that do not satisfy the conditions of Theorem 2 but where the

observability-based planner π^o still generates collision-free paths.

Figure 10 (b) plots the percentage of runs where the MAV reached the goal versus the minimum distance for the two cases. The percentage increases as the minimum distance between obstacles increases. When the minimum distance is greater than 80 meters for the case with measurement uncertainties or when the minimum distance is greater than 70 meters for the case with perfectly known obstacle locations, the MAV is always maneuvered to the goal using the observability-based planner. In addition, the percentage for all the environments with the minimum distance from 10 to 100 meters for both cases is nonzero. Accordingly, the minimum distance $2V\tau^l = 104$ m, which satisfies the goal reaching conditions of Theorem 3 for the switching algorithm, is not necessary for the observability-based planner π^o to achieve goal reaching performance.

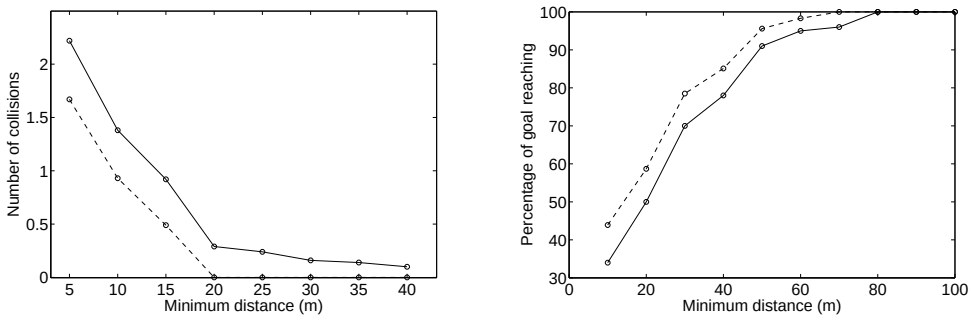

(a) (b)

Figure 10: This figure shows the statistical performance of the observability-based planning algorithm implemented in the environments with varying minimum distance between obstacles for the cases with the standard deviation of the bearing measurement noise 2° and with perfectly known obstacle locations. Subfigure (a) plots the average number of collisions over 100 simulation runs versus the minimum distance between obstacles. Subfigure (b) plots the percentage of runs where the MAV reached the goal versus the minimum distance.

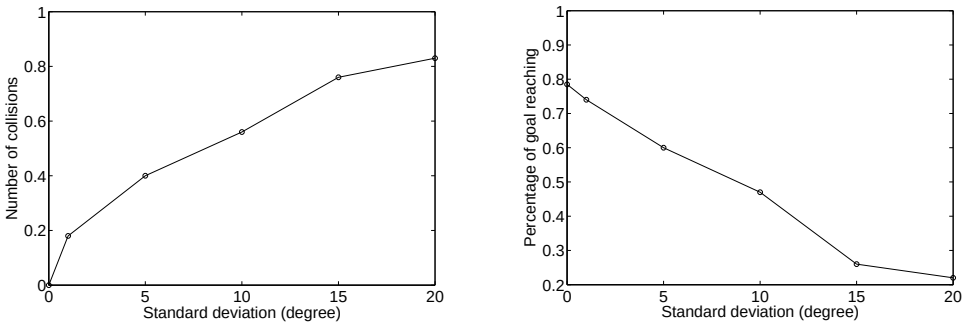

(a) (b)

Figure 11: This figure shows the statistical performance of the observability-based planning algorithm with varying measurement uncertainties in the environment with the minimum distance 30 meters. Subfigure (a) plots the average number of collisions over 100 simulation runs versus the standard deviation of the bearing measurement noise. Subfigure (b) shows the percentage of runs where the MAV reached the goal versus the standard deviation.

To take into account the effect of measurement uncertainties, Monte Carlo simulations were also conducted to test the performance of the algorithm π^o with varying measurement uncertainties. Similarly, we evaluate the number of collisions and the percentage of runs for the MAV to reach the goal. Figure 11 plots the average number of collisions over 100 simulation runs and the percentage of runs where the MAV reached the goal versus the standard deviation of the bearing measurement noise for the environment with the minimum distance 30 meters. Based on the figure, as the standard deviation of the measurement noise increases, the number of collisions increases and the percentage of runs where the MAV reached the goal decreases.

6. Conclusions

This paper presents an observability-based planning algorithm using bearing-only measurements. We perform a nonlinear observability analysis for state

estimation and argue that collision avoidance and uncertainty minimization problems are complementary. Based on this analysis, we design a cost function that minimizes the estimation uncertainties while simultaneously avoiding obstacles. By minimizing the cost function, the path planning algorithm is developed directly in the local-level frame. We use a look-ahead policy to plan optimal paths over a finite time horizon. The performance of the planning algorithm is analyzed and the characteristics of the environments in which the planning algorithm guarantees collision-free paths that lead to a goal configuration are described. Numerical results show that the observability-based planning algorithm is successful in solving the single and multiple obstacle avoidance problems while improving the estimation accuracy.

7. Acknowledgement

This research is supported by OSD and AFRL under contract FA8650-08-C-1411 and is partially funded by the AFRL Munition Directorate, Eglin AFB.

References

[1] B. Call, Obstacle avoidance for unmanned air vehicle using computer vision, Master's thesis, Brigham Young University (December, 2006).

[2] A. Curtis, Path planning for unmanned air and ground vehicles in urban environments, Master's thesis, Brigham Young University (2008).

[3] E. Frazzoli, M. Dahleh, E. Feron, Real-time motion planning for agile autonomou vehicles, Journal of Guidance, Control and Dynamics 25 (2002) 116–129.

[4] Y. Watanabe, E. Johnson, A. Calise, Vision-based approach to obstacle avoidance, in: Proceedings of the AIAA Guidance, Navigation, and Control Conference and Exhibit, 2005.

[5] A. Pongpunwattana, R. Rysdyk, Real-time planning for multiple autonomous vehicles in dynamics uncertain environments, AIAA Journal of Aerospace Computing, Information, and Communication 1 (2004) 580–604.

[6] K. Sedighi, K. Ashenayi, R. Wainwright, H. Tai, Autonomous local path planning for a mobile robot using a genetic algorithm, Congress on Evolutionary Computation 2 (June 2004) 1338–1345.

[7] J. Latombe, Robot Motion Planning, Kluwer Academic Publishers, Boston, MA, 1991.

[8] H. Yu, R. Beard, J. Byrne, Vision-based local multi-resolution mapping and path planning for miniature air vehicles, in: Proceedings of American Control Conference, 2009.

[9] H. Yu, R. Beard, J. Byrne, Vision-based local multi-resolution path planning and obstacle avoidance for micro air vehicles, in: Proceedings of the AIAA Guidance, Navigation and Control Conference, 2009.

[10] H. Yu, R. Beard, J. Byrne, Vision-based navigation frame mapping and

planning for collision avoidance for miniature air vehicles, Special Issue on Aerial Robotics, Control Engineering Practice 18 (7) (2010) 824–836.

[11] R. Hermann, A. Krener, Nonlinear controllability and observability, IEEE Transactions on Automatic Control 22 (5) (1977) 728–740.

[12] Y. Song, J. W. Grizzle, The extended Kalman Filter as a local asymptotic observer for descrete -time nonlinear systems, Journal of Mathemetical Systems, Estimation, and Control 5 (1995) 59–78.

[13] A. Martinelli, R. Siegwart, Observability analysis for mobile robot localization, in: Proc. IEEE/RSJ International Conference on Intelligent Robots and Systems (IROS 2005), 2005, pp. 1471–1476. doi:10.1109/IROS.2005.1545153.

[14] I. Rhee, M. Abdel-Hafez, J. Speyer, Observability of an integrated GPS/INS during maneuvers 40 (2) (2004) 526–535. doi:10.1109/TAES.2004.1310002.

[15] T. Vidal-Calleja, M. Bryson, S. Sukkarieh, A. Sanfeliu, J. Andrade-Cetto, On the observability of bearing-only SLAM, in: Proc. IEEE International Conference on Robotics and Automation, 2007, pp. 4114–4119. doi:10.1109/ROBOT.2007.364111.

[16] M. Bryson, S. Sukkarieh, Observability analysis and active control for airborne SLAM, IEEE Transactions on Aerospace and Electronic Systems 44 (1) (2008) 261–280. doi:10.1109/TAES.2008.4517003.

[17] H. Yu, R. Sharma, R. Beard, C. Taylor, Observability-based local path planning and collision avoidance for micro air vehicles using bearing-only

measurements, in: Proceedings of IEEE American Control Conference, 2011.

[18] MathWorks, Optimization Toolbox, http://www.mathworks.com.

[19] R. W. Beard, T. W. McLain, Small Unmanned Aircraft: Theorey and Practice, Princeton University Press, 2012(to appear).